Food and Chemical Toxicology 123 (2019) 374–384

Contents lists available at ScienceDirect

Food and Chemical Toxicology

journal homepage: www.elsevier.com/locate/foodchemtox

Molecular signatures of cytotoxic effects in human embryonic kidney 293 cells treated with single and mixture of ochratoxin A and citrinin

Liang Gong[a,1], Hong Zhu[a,1], Taotao Li[a,1], Guangfeng Ming[b], Xuewu Duan[a,*], Jiasheng Wang[c], Yueming Jiang[a]

[a] Key Laboratory of Post-Harvest Handling of Fruits, Ministry of Agriculture/ Guangdong Provincial Key Laboratory of Applied Botany, South China Botanical Garden, Chinese Academy of Sciences, Guangzhou, 510650, China
[b] Department of Critical Care Medicine, Xiangya Hospital, Central South University, Changsha, 410008, China
[c] Department of Environmental Health Science, College of Public Health, University of Georgia, Athens, 30602, USA

ARTICLE INFO

Keywords:
Ochratoxin A
Citrinin
Cell apoptosis
Cell cycle
HEK293 cells
Nephrotoxicity

ABSTRACT

Ochratoxin A (OTA) and citrinin (CTN) are important mycotoxins, which often coexist in food and feed stuff. In this study, individual and combinative cytotoxicity of OTA and CTN were tested in human embryonic kidney (HEK) 293 cells via MTT assay, and synergistic cytotoxic effects were found following co-treatment with OTA and CTN, manifested by significant accumulation of HEK293 cells in S and G2/M stages. Transcriptomic and sRNA sequencing were performed to explore molecular signatures mediating individual or combinative cytotoxicity. A total of 378 miRNAs were identified, among which 66 miRNAs targeting thousands of genes were differentially expressed in response to different treatments, and 120 differentially expressed genes (DEGs) were regulated by either individual or combinative treatments. Correlations between two representative miRNAs (hsa-miR-1-3p and hsa-miR-122–5p), and their target genes, *programmed cell death 10* (*PDCD10*) and *cyclin G1* (*CCNG1*), associated with apoptotic signaling and cell cycle were analyzed by luciferase assay system. Further, their expression patterns were validated by quantitative real-time PCR and western blot analysis, suggesting that both miRNA-target interactions might account for the mycotoxin-induced cell death. Taken together, these findings provide molecular evidences for synergistic cytotoxic effects of exposure to single and mixture of OTA and CTN in HEK293 cells.

1. Introduction

Ochratoxin A (OTA), a natural mycotoxin mainly produced by *Aspergillus ochraceus* and *Penicillium verrucosum*, naturally occurs in many commodities from grains to coffee beans worldwide (IARC, 1993). OTA is a potent toxicant that can induce nephrotoxic, hepatotoxic, embryotoxic, neurotoxic, immunotoxic, genotoxic, and carcinogenic effects in many *in vitro* and *in vivo* models (Heussner and Bingle, 2015; Ostry et al., 2013; Pflaum et al., 2016), and has been classified as a group 2B compound with possibly carcinogenic to humans (IARC, 1993). OTA has been associated with Balkan endemic nephropathy in humans and pigs (IARC, 1993; Tao et al., 2018). The mechanisms underlying OTA nephrotoxicity include inhibition of protein synthesis, DNA damage, cell cycle arrest, cell apoptosis, and so on (Reddy and Bhoola, 2010; Schilter et al., 2005).

Citrinin (CTN), mainly produced by *P. citrinum* and *P. verrucosum*, has been found to naturally occur in cereal grains, such as wheat, barley, corn, and rice (de Oliveira Filho et al., 2017). CTN is a potent nephrotoxin and causes kidney damage in laboratory animals similar to swine nephropathy (Kumar et al., 2007). CTN induced the formation of micronuclei and chromosome/chromatid breaks, as well as the interruption of the spindle formation and tubulin polymerization in various cell cultures (Chang et al., 2011; Donmez-Altuntas et al., 2007).

Co-contamination of OTA and CTN has been commonly found in

Abbreviations: BAK1, BCL2-antagonist/killer 1; BCL2L12, BCL2-like 12 (proline rich); CCNG1, cyclin G1; CDC, cell division cycle; CDK1, cyclin-dependent kinase; CDKN1B, cyclin-dependent kinase inhibitor 1B; CTN, citrinin; DEGs, differentially expressed genes; FDR, false discovery rate; GAPDH, glyceraldehyde-3-phosphate dehydrogenase; GO, Gene Ontology; HEK, human embryonic kidney; *KEGG*, Kyoto Encyclopedia of Genes and Genomes; NGS, Next generation sequencing; OTA, ochratoxin A; PAGE, poly-acrylamide gel electrophoresis; PDCD10, programmed cell death 10; RPM, reads per million mapped reads; RT-qPCR, Real-time quantitative PCR

* Corresponding author.
E-mail address: xwduan@scbg.ac.cn (X. Duan).
[1] Those authors contributed equally to this work.

https://doi.org/10.1016/j.fct.2018.11.015
Received 29 May 2018; Received in revised form 26 October 2018; Accepted 7 November 2018
Available online 11 November 2018
0278-6915/

cereal components and grain products, partially because the toxigenic *P. verrucosum* can produce both mycotoxins, and CTN concentrations found in grains are often several times higher than co-existing OTA (Wawrzyniak and Waskiewicz, 2014; Pleadin et al., 2018). Several studies have revealed synergistic effects of CTN in combination with OTA. For example, co-exposure to OTA and CTN led to synergistically interaction on inducing cytotoxicity in HepG2 hepatocytes (Gayathri et al., 2015); co-treatment with CTN and OTA synergistically reduced glutathione and induced the expression of *Hsps* in porcine kidney PK15 cells (Klaric et al., 2014). Considerable efforts have been made to understand toxic mechanisms for combinative toxicity of OTA and CTN, and found that CTN induced the expression of cyclooxygenase-2 that can promote OTA transforming into a genotoxic compound; in addition, CTN could increase oxidative and inflammatory stress, which can increase OTA-DNA adduct formation and genotoxic effects (Malir et al., 2016; Wu et al., 2011). Although co-treatment with CTN and OTA synergistically induced nephrotoxicity and apoptotic cells in rabbits (Kumar et al., 2014), their molecular mechanism for interactions is largely unknown, and warrants further studies.

miRNAs are found to play a central role in posttranscriptional regulation of gene expression involved in numerous biological processes in eukaryotes (Vidigal and Ventura, 2015). They are processed from short hairpin precursors and regulate endogenous target genes to impact development and stress responses (Saraiva et al., 2017). The evolution of miRNAs and their targets represents one of the most dynamic circuits, and it is estimated that miRNAs can regulate more than half of the protein-coding genes in human (Bartel, 2009), and moreover, a considerable number of miRNAs have been implicated in various human diseases, including kidney diseases (Huang et al., 2015). Dai et al. (2014) reported 409 known miRNAs and eight novel miRNAs involved in rat kidneys with OTA-induced nephrotoxicity, and the differentially expressed miRNAs were closely associated with MAPK signaling pathway. However, little is known regarding the linkage between miRNAs and synergistic nephrotoxicity induced by co-exposure to OTA and CTN.

Next generation sequencing (NGS) provides an effective approach for exploring transcriptomic data with advantages in resolution, robustness and inter-lab portability. Comparative transcriptome analysis has been successfully performed to explore candidate genes in multiple species, including animals and humans, for example, transcriptome analysis was performed for HepG2 cells treated with OTA and 2726 genes were found with significantly different expression levels (Zhang et al., 2016). Nowadays, with the rapid development of NGS technologies and bioinformatics tools, RNA-sequencing technique has become the most powerful tool for transcriptomic data mining, and more miRNAs and target genes have been identified in a wider range of species, presenting an extensive platform for comparative analysis.

The purpose of this study is to explore the molecular mechanisms underlying toxic effects on individual exposure to OTA or CTN and combinative cytotoxic effects on co-exposure to OTA and CTN in human embryonic kidney (HEK) 293 cells via NGS approaches. A great number of differentially expressed miRNAs and corresponding genes were identified, and the correlations between miRNAs and their target genes associated with cell cycle and apoptotic signaling were further analyzed. Our results provide critical molecular basis for understanding OTA and CTN-induced synergistic cytotoxicity in the HEK293 cells.

2. Materials and methods

2.1. Chemicals and reagents

HEK293 cells was purchased from the distributing agent of ATCC (American Type Culture Collection) in China (Beijing Zhongyuan Ltd.). Ochratoxin A (OTA) and Citrinin (CTN) were purchased from Sigma-Aldrich™ (St Louis, OM, USA). Anti-PDCD10 (#LS-C265842) and anti-CyclinG1 (#sc-8016) were purchased from *LifeSpan* ™ (Seattle, WA, USA). Anti-GAPDH was purchased from KangChen Bio-tech Inc (Shanghai, China). All other reagents were all of analytical grade and purchased from Guangzhou JY Chemicals Co., Ltd (Tianhe District, Guangzhou, China).

2.2. MTT assay

Individual and combined cytotoxicity of OTA and CTN were determined, respectively, using the MTT test, which is a colorimetric assay for assessing viable cells through converting MTT into its insoluble formazan underlying the mitochondrial succinate dehydrogenase (Berridge et al., 2005). HEK293 cells were cultured in DMEM with 10% FBS and 1% penicillin/streptomycin in a humidified incubator with 5% CO2 at 37 °C, and then seeded in 96-well plates at the density of 8×10^3 cells/well, and incubated for 24 h at 37 °C and 5% CO_2, then treated with OTA or CTN and/or OTA + CTN combined with equimolar doses, ranging from 0.2 to 450 μM, diluted from the stock solution (10 mg/mL), till 48 h. After that, the assay was conducted according to manufacture protocols of MTT cell proliferation and cytotoxicity assay kit (Beyotime, China). The absorbance was measured by SpectraMax microplate reader (Molecular Devices, California, USA) at a wavelength of 560 nm. Blank group and solvent group (25% ethanol in 0.01M PBS) were used as negative controls. IC_{50} value, the concentration causing 50% loss of cell viability, was generated according to the cell viability data.

2.3. Cell cycle analysis

Detection of cell cycle in HEK293 cells treated with the IC_{50} value of OTA and CTN (individual or combined, respectively) was performed by flow cytometry (Accuri C6 flow cytometer, BD Biosciences, NJ, USA). HEK293 cells were cultured in 6-well plates at density of 5×10^4 cells/well, and incubated for 24 h. Then, the mycotoxins were added to the cultures, after 48 h, the cells were washed by trypsin in 0.25% EDTA and suspended by fresh medium. The suspended cells were collected by centrifugation for 4 min at 2000 rpm, then washed once by pre-cooled PBS (phosphate buffered saline) and stored in 70% ethanol for overnight at 4 °C. After that, the cells were collected and suspended in 500 μl PBS, then stained by PI solution (Sigma, MO, USA). The samples were transferred to the flow cytometer to measure the cell fluorescence.

2.4. RNA extraction and illumina sequencing

HEK293 cells were cultured and treated with the concentration of IC_{50} value of OTA and CTN (individual or combined, respectively) for 48 h, and then were collected for total RNA extraction using trizol reagents (Thermo Fisher Scientific, Waltham, MA, USA). The quantity and quality of the total RNA were assessed by a NanoDrop 2000 UV–Vis Spectrophotometer (Thermo Scientific, USA). Two replicates for each treatment were collected respectively, and RNA was frozen in liquid nitrogen immediately and then stored at −80 °C.

Total RNA was extracted from the two sets of cells, respectively, with Total RNA Isolation System (Promega, USA). For RNA-seq, equivalent quantities of total RNA isolated from different sets were prepared. After the DNase I treatment, magnetic beads with Oligo (dT) were used to isolate mRNA. Mixed with the fragmentation buffer, the mRNA is fragmented into short fragments. Then cDNA is synthesized using the mRNA fragments and random hexamer primers. For QC steps, Agilent 2100 Bioanaylzer and ABI StepOnePlus Real-Time PCR System are used in quantification and qualification of the sample library. The libraries were sequenced by Illumina HiSeq™ 2000 at Ribobio, with a read length of 100 bp. Reads with adaptors or unknown nucleotides larger than 5% were removed from the raw reads and low quality reads have also been discarded. All the raw data were deposited in National Center for Biotechnology Information with the accession number: SRP129578.

2.5. Screening of differentially expressed genes (DEGs)

The RPKM (Reads Per kb per Million reads) method was used to compare gene expression levels between transcriptome sequences from different sets (Verma et al., 2013). DEGs between any two samples were identified and analyzed on the Ribobio's computation platform (Guangzhou, China) employing a strict algorithm developed from the significance of digital gene expression profiles. The statistical test results were corrected for multiple testing with the Benjamini-Hochberg false discovery rate (FDR). Sequences were selected as significant DEGs if the FDR ≤ 0.001, and fold change > 2 between any two comparisons.

2.6. Gene Ontology (GO) classification of DEGs and pathway analysis

All DEGs were mapped to each term of Gene Ontology database, and significantly enriched GO terms were found in DEGs compared to the genome back-ground, taking the corrected-p value (FDR) ≤ 0.05 as a threshold (Huntley et al., 2015). Enrichment analysis (Fisher's Exact Test) was performed in Blast2GO to test the significance of enrichment of selected gene families. To identify significantly enriched metabolic pathways or signal transduction pathways with DEGs, KEGG (Kyoto Encyclopedia of Genes and Genomes) pathway analysis was performed with q-value ≤ 0.05 as the criteria for pathway selection (Kanehisa et al., 2017).

2.7. Small RNA-seq and data processing

For microRNA sequencing, small RNAs with the size between 18 and 30 nt were excised from approximately 15 μg of total RNA isolated by poly-acrylamide gel electrophoresis (PAGE). The sequencing libraries were constructed by a Small RNA Library Preparation kit (Illumina Inc., San Diego, CA, USA) according to the manufacturer's protocol. Each library was barcoded with different indices and stored at −80 °C before sequencing. Sequencing was performed on an Illumina HiSeq2500 sequencer, generating SE: 1 × 50bp reads. All sequencing data were deposited in the NCBI GEO (accession number GSE93148).

2.8. miRNA identification

The sequencing reads were processed to remove 3′ and 5′ adaptors, and cleaned by Q30 value. Reads with > 20% bases < Q30, and N base > 10% were filtered. The remaining reads were further filtered if read length was > 46 bp or < 17 bp. The derived reads were mapped to various RNA database including Silva, GtRNAdb, Rfam, and Repbase by Bowtie (Langmead et al., 2009) for annotation. The unannotated reads containing small regulatory RNAs were processed for miRNA identification by miRDeep2 (Friedlaender et al., 2012). The secondary structure and mapping information was processed as described in the miRDP package (Yang and Li, 2011). The precursors were aligned to short reads, and statistical analyses of read distributions were generated for each miRNA gene for evaluation of miRNA. The miRDeep2 output figures were manually checked by the existence of miRNA* sequences, and the precision of editing of mature sequences. To quantify the abundance of miRNA, the RPM value was defined as 'reads per million mapped reads' (Fahlgren et al., 2007). New miRNA prediction was performed by Mireap software (https://sourceforge.net/projects/mireap/). The miRNA targets were annotated by standard settings of psRNATarget (Dai and Zhao, 2011) with maximum expectation value 3.0.

To analyze differential expression of miRNAs, DESeq2 software was used, and expression fold change > 2 and a [Benjamini–Hochberg false discovery rate (FDR) corrected] P-value < 0.01 were selected (Love et al., 2014). The miRNA expression data were normalized by the row z-score method. Hierarchical clustering of gene expression was performed by the clustergram function in the Matlab Bioinformatics toolbox with minor changes. GO enrichment analysis was performed as previously described, and visualized using the ReviGO tool (Supek et al., 2011).

2.9. Real-time quantitative PCR (RT-qPCR) and western blot analysis

In order to detect the expression of selected differentially expressed genes and miRNAs in HEK293 cells treated with the IC_{50} value of individual and combined OTA and CTN, The primers of candidate miRNAs were designed by PrimerExpress 2.0 with default settings (Table S1). RT-qPCR was performed using the CFX96 Touch™ with iQTM SYBR® Green Supermix (Bio-Rad, CA, USA). Briefly, 500 ng of purified RNA was reverse transcribed using mature miRNA-specific primers and miRNA qPCR Starter Kit (RIBOBIO, Guangzhou, China). The following conditions were used for amplification: 95 °C for 20 s, 40 cycles of PCR amplification at 95 °C for 10 s, 60 °C for 30 s and 70 °C for 1 s β-Actin was used as the house keeping gene according to Farabegoli et al. (2017) for validation of different expressed genes while U6 was used as internal controls to normalize miRNA in different samples with the $2^{\Delta\Delta Ct}$ method (Livak and Schmittgen, 2001).

HEK293 cells were cultured and treated as described above and then scraped into cell lysis solution (Thermo Scientific, Waltham, MA, USA). The cell lysates were prepared by centrifugation at 17500 (× g) for 15 min. Twenty micrograms of proteins were denatured by incubation at 95 °C for 5 min in 5 × SDS-PAGE buffer. Then they were separated by 10% SDS-PAGE and transferred onto PVDF membrane (Amersham Pharmacia Biotech, Uppsala, Sweden). The membrane were blocked in 10% skimmed milk, and incubated overnight at 4 °C with the specific antibodies for anti-PDCD10 and anti-CyclinG1, respectively, then washed 3 times with TBST (10 mM Tris, 100 mM NaCl, 0.1% Tween-20) every 5 min. After washing with TBST, membranes were then incubated with the secondary antibodies of GAPDH at 1:10000 dilution for 1 h. The immunoreactive bands were visualized by using Odyssey Infrared Imaging System (LI-COR, Lincoln, NE).

2.10. Dual-luciferase reporter assay

Construction of dual luciferase plasmid was performed by the vector of pmiR-RB-REPORT™ (Promega, WI, USA) harboring the 3′ UTR of the PDCD10 and CyclinG1, respectively. The sequences of the miRNA mimics and negative control were designed and procured from RIBOBIO (RIBOBIO, Guangzhou, China). The experimental procedure was based on the manufacturer's introductions of Dual-Glo® luciferase assay system (Promega, WI, USA). MiRNA mimics (50 nM) and reporter construct (250 ng per well) were co-transfected into the HEK293 cells using Lipofectamine™ 2000 (Invitrogen, CA, USA). The activity of the firefly and *Renilla* luciferases was determined using a fluorescent light meter (Veritas 9100–002). Based on the results of wild-type gene, mutants (PDCD10-3'UTR-Mut and CyclinG1-3'UTR-Mut) were cloned into the same vector for further verification of the inhibitory effects of hsa-miR-1-3p and hss-miR-122–5p on their corresponding target genes. All primers used are listed in Table S1.

3. Results

3.1. Cytotoxicity of OTA and CTN to HEK293 cells

As shown in Fig. 1, both OTA at the test concentration ranging from 0 to 30 μM and CTN at the test concentration ranging from 0 to 450 μM caused notable cytotoxic effects on HEK293 cells in a dose-dependent manner. OTA induced higher reduction in the viability of HEK293 cells than that induced by CTN, as shown by the IC_{50} of OTA at around 16 μM, and the IC_{50} of CTN at 189 μM. Co-treatment of OTA/CTN at the equimolar concentrations ranging from 0 to 30 μM showed an increased cytotoxicity in HEK293 cells with the IC_{50} of 7 μM, indicating that the combinative cytotoxic effect tends to be synergistic.

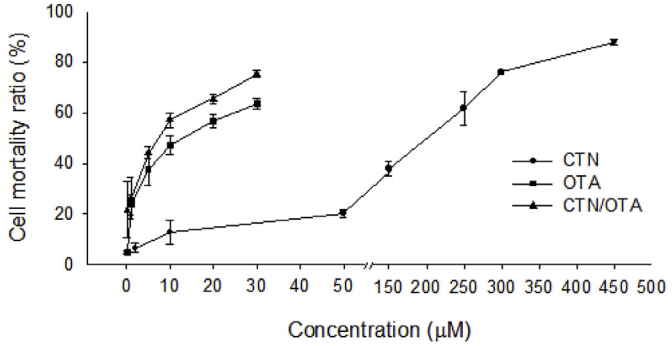

Fig. 1. Cytotoxic effects of CTN and OTA (individually and combined) on human embryonic kidney 293 cells. Data are calculated as mean values ± SD of the independent experiments (n = 3).

Table 1
Cell cycle analysis of HEK293 cells treated by mycotoxins.

Treatments	G0/G1 (%)	S (%)	G2/M (%)
Blank group	60.55 ± 0.69	19.19 ± 1.8	16.06 ± 1.6
Solution group	60.01 ± 1.0	18.52 ± 1.2	17.86 ± 0.95
CTN (189 μM)	47.48 ± 1.9	17.53 ± 1.2	34.02 ± 1.3
OTA (16 μM)	51.15 ± 1.4	29.48 ± 1.1	15.48 ± 0.8
CTN + OTA (7 μM)	45.55 ± 1.6	30.5 ± 0.8	20.76 ± 1.6

3.2. Cell cycle arrest

Normal cell cycle is very important for cell division and cell growth. As shown in Table 1, OTA treatment resulted in a statistically significant S phase arrest rate (29.48%) in HEK293 cells, as compared to the rates in the blank group (19.19%) and solvent group (18.52%). CTN treatment caused a significant accumulation of the HEK293 cells at G2/M stage with the rate (34.02%), as compared to the solvent group (17.86%) and blank group (16.06%), respectively. Co-treatment of OTA and CTN caused significant increase at S phase (30.5%) and G2/M stage (20.76%), as compared to the solvent group.

3.3. Sequencing and annotation analysis for transcriptome data

Each generated datum is more than 92.15% in clean rate and the Q20 value is greater than 97.41% (Table S2). On average, approximately 14 million effective pair-end reads were obtained for each library by Illumina HiSeq (2000) sequencing. After data filtering and stringent quality check, more than 80% of the effective reads were mapped to human genome assembly and most of these mapped reads only had a single mapping locus. It was also found that a higher percentage of reads were mapped to '-' strand than to '+' strand. All these reads were used for further analysis (Table S3).

DEGs between control and different treatment protocols were screened with thresholds fold change > 2 and FDR ≤0.05. Over two thousand genes were found to differentially express between control and OTA-treated samples, and nearly five times genes were down-regulated (1769) than up-regulated (361). Similar patterns were found between control and CTN/OTA co-treated samples, but with less DEGs. However, much fewer DEGs were identified for CTN -treated samples as compared to control, and most of them were up-regulated (Fig. 2a–c). In addition, Venn diagrams was used to assemble the DEGs underlying treatment protocols (Fig. 2d), and found that only 120 DEGs was commonly regulated. These results indicate that treatment or co-treatment with OTA and CTN induces cytotoxic response partly through similar molecular pathways.

GO analysis was performed based on NR annotation. It provides a distinct classification of gene products in terms of molecular functions, cellular components and biological processes. Under biological processes, 15, 46, and 24 GO terms were identified, and were significantly enriched ($p < 0.01$) in CTN-treated, OTA-treated, and CTN/OTA co-treated samples (Table S4), respectively. The top five most statistically relevant GO functional groups was shown in Table 2, in which it is clearly suggested that programmed cell death (PCD) and cell cycle are the tightly regulated biological processes of HEK293 underlying treatment protocols. To further understand how different treatment protocols affect HEK293 cells at the molecular level, we mapped the DEGs to the terms in KEGG database. By comparing with the whole genome background, we identified significantly ($p < 0.01$) enriched classifications, as shown in Fig. S1.

3.4. Identification of genes related to programmed cell death and cell cycle

Of the genes involved in programmed cell death, 81, 221 and 121 genes were differently expressed in CTN-treated, OTA-treated and CTN/OTA co-treated samples (Table S5), respectively. In the case of apoptosis, as one form of programmed cell death, most apoptosis-related genes were up-regulated in response to CTN. For some details (Fig. S2), most *TNFR* related genes (*TNFAIP1, TNFRSF1A* and *TNFRSF12A*) were down-regulated in response to OTA treatment, whereas in CTN/OTA co-treated samples, *TNFRSF1A* was identified with down-regulation and *TNFRSF10D* with up-regulation, these results were further confirmed by qPCR. Our qPCR results also showed that *TNFRSF12A* and *TNFAIP1* were down-regulated in CTN/OTA co-treated samples. Meanwhile, the programmed cell death 4 (*PDCD4*), and apoptosis-related cysteine peptidase (caspase 2, CASP2) were down-regulated in OTA-treated samples, which was accordance with the qPCR results. According to qPCR results, *PDCD4* and *CASP2* were also down-regulated in CTN and CTN/OTA co-treated samples. Additionally, *Bcl-2* gene encoding autophagy regulator also showed different expression pattern in response to different treatment protocols. *BCL2-antagonist/killer 1* (*BAK1*) and *BCL2-like 12 (proline rich)* (*BCL2L12*) were significantly down-regulated in OTA-treated samples. In CTN/OTA co-treated samples, *BAK1* was down-regulated. Additionally, A *BCL2-associated athanogene 3* (*BAG3*) gene was also identified with down-regulation while *BAK1* and *BCL2L12* with up-regulation in CTN-treated samples according to qPCR results (Fig. S2). There were 25, 88 and 60 Cell cycle-related genes showed different expression patterns in relation to CTN-treatment, OTA-treatment, and CTN/OTA co-treatment, respectively (Table S6). In contrast, 7 cell division cycle-related genes (*CDC25A, CDC7, CDC25C, CDC26, CDC6, CDC23* and *CDC34*) were down-regulated in OTA-treated samples. For CTN/OTA co-treated samples, two cell division cycle related genes (*CDC7*) was down-regulated. It is consistent both RNA-Seq and qPCR results. However, our qPCR results also found the down-regulation of genes (*CDC7, CDC25C, CDC26, CDC6, CDC23* and *CDC34*) in CTN-treated samples. For cell cycle phase transition, cyclin-dependent kinase inhibitor 1B (*CDKN1B*) was down-regulated in CTN-treated sample, while it was up-regulated in OTA-treated and CTN/OTA co-treated samples, which is consistent with qPCR results. Additionally, the expression of cyclin (*CCNB1* and *CCNE1*) and cyclin-dependent kinase (*CDK1*) were down-regulated in OTA-treated samples. These gene expressions were further confirmed by qPCR with the consistent results (Fig. S2).

3.5. sRNA sequencing and miRNA profiling of mycotoxin-treated cells

In order to identify microRNAs and their expression patterns in HEK293 cells in response to treatment protocols, eight small RNA libraries from control, CTN-treated, OTA-treated, and CTN/OTA co-treated samples were constructed and sequenced. For each individual mycotoxin-treated sample, the retrieved raw reads ranged between 10.8 million and 27.3 million (Table S7) with focus on reading lengths from 17 to 46 bp, and mapped them to miRBase v.21, Rfam 11.0, UCSC and pirnabank databases to annotate the composition of the small RNA population (Table S7). In total, > 118 million raw reads were obtained

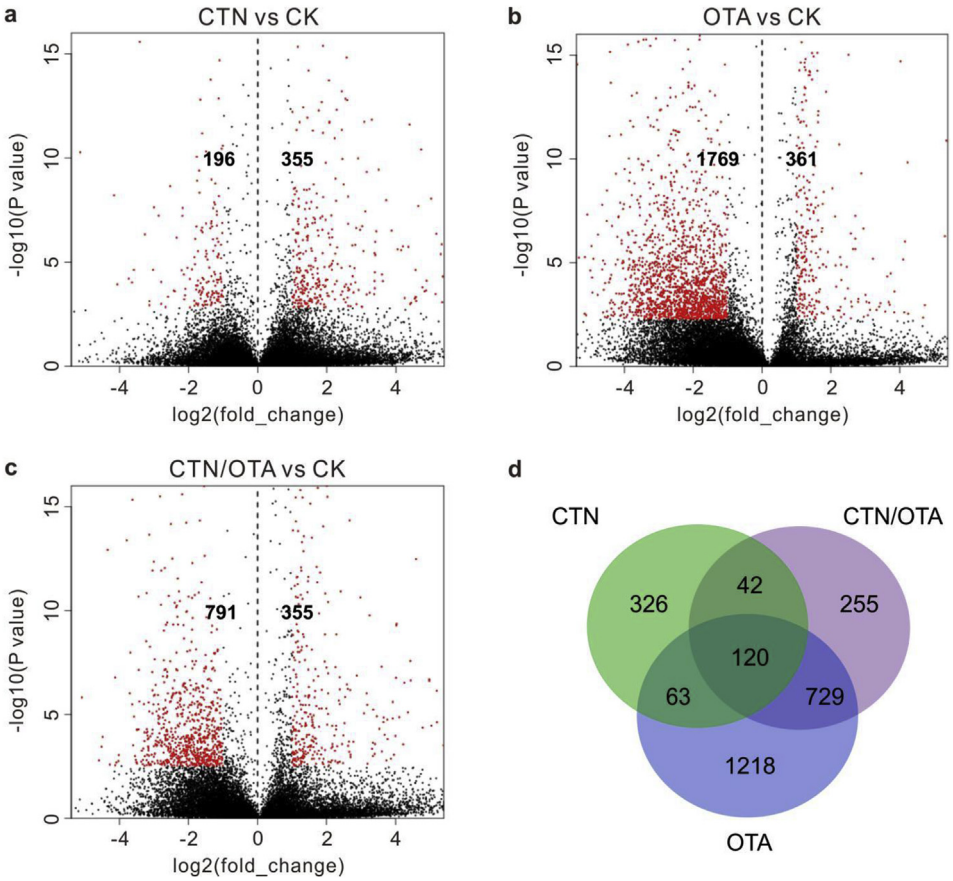

Fig. 2. Effects of CTN and OTA (individually and combined) on gene expression of human embryonic kidney 293 cells. (a) Volcano of significantly different expressed genes (red colour) between control and CTN. (b) Volcano of significantly different expressed genes (red colour) between control and OTA. (c) Volcano of significantly different expressed genes (red colour) between control and CTN/OTA. (d) A Venn diagram comparing significantly different expressed genes upon different toxin treatments. (For interpretation of the references to colour in this figure legend, the reader is referred to the Web version of this article.)

Table 2
Top five most statistically functional categories induced by individual or combined exposure of CTN and OTA.

Gene Ontology Group	Gene number	Corrected p-value
CTN		
response to topologically incorrect protein	18	4.11E-3
response to unfolded protein	17	5.42E-3
protein folding	20	8.72E-3
programmed cell death	81	2.42E-2
cell death	88	2.42E-2
OTA		
RNA processing	151	1.25E-10
cell cycle	258	7.87E-08
ribonucleoprotein complex biogenesis	70	5.90E-07
RNA splicing	83	6.84E-07
cellular macromolecule metabolic process	920	2.79E-06
CTN/OTA		
DNA metabolic process	107	6.86E-06
mitotic cell cycle	100	6.95E-06
cellular response to DNA damage stimulus	80	5.61E-05
cell cycle	146	7.07E-05
RNA processing	77	2.57E-4

and over 26 million reads were processed for miRNA identification.

By mapping sequences from all treated samples against all known miRNAs in miRBase v.21 and removing those with read number less than 10, a total of 26,359,376 reads were retrieved. After further retaining reads found in both replicates for each treatment, 378 miRNAs belonging to 249 conserved miRNA families were obtained. Among these, a total of 356, 324, 324 and 321 conserved miRNAs (belonging to 231, 216, 214, and 210 families) were identified from control, CTN-treated, OTA-treated, and CTN/OTA co-treated samples, respectively. We found that 285 conserved miRNAs belonging to 187 families as commonly expressed in all samples (Fig. S3). In addition, we found that 25 miRNAs whose expression was completely suppressed by treatment protocols (Table S8). The read abundance of all the known miRNA family members were normalized, as reflected by RPM (reads per million mapped reads), which showed a great variation among families in all treated samples (Table S8). The highest read abundance (151,519 RPM) was detected for mir-10 family, which was 2–13 times more than other relatively abundant miRNA families, including mir-30, mir-148, mir-218, and so on, with their total read abundance ranged from 10,000 to 60,000 RPM. Lower expression (between 1000 and 10,000 RPM) was observed for 37 miRNA families, including mir-221, mir-101, mir-191, etc. All the remaining 198 miRNA families were lowly expressed with their total read abundance less than 1000 RPM (Fig. S3, Table S8).

Mireap core algorithms (https://sourceforge.net/projects/mireap/) were implemented for the discovery of the new miRNAs, using a set of criteria such as low minimal free energy for hairpin structure of its precursor, detection of a miRNA* strand, and location of intergenic region (Li et al., 2012). For those prediction with a read abundance cut-off of 10 and high probability, a total of 433 potential novel miRNA candidates were identified, deriving from intergenic regions with conventionally and stable secondary structure. These novel miRNA candidates were lowly expressed, compared to the conserved miRNAs; only less than 15% of them had a read abundance greater than 100 RPM (Table S9).

3.6. Differentially expressed miRNAs upon mycotoxin treatment

MiRNAs are usually expressed in a temporal- and spatial-specific manner, thereby greatly contributing to specific profiles of gene and protein expression. To explore the roles of miRNAs upon treatment protocols, quantification of miRNAs was performed in each treatment protocol and obtained 66 significantly differentially expressed miRNAs (DEmiRs) among treatment samples ($p < 0.01$, Fig. 3a, Table S10).

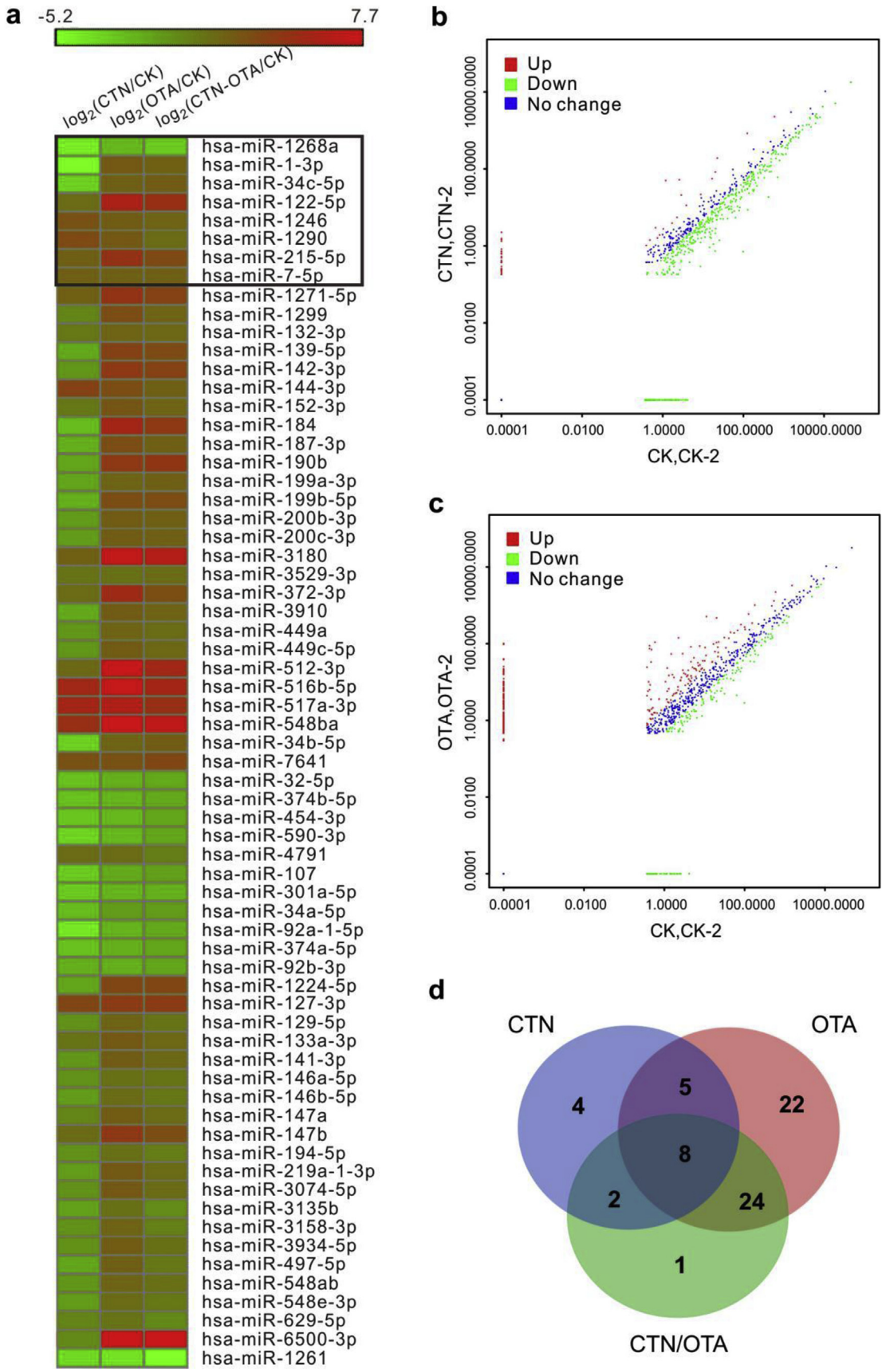

Fig. 3. Analysis of miRNA expression in mycotoxin-treated human embryonic kidney 293 cells. (a) A heatmap of differentially expressed miRNAs (DEmiRs) upon CTN and OTA treatments. Black box indicates the DEmiRs for all toxin treatments (individually and combined). (b–c) The trend of expression change of all identified DEmiRs upon CTN and OTA treatments. (d) A Venn diagram showing the numbers of common and toxin-specific DEmiRs.

Around 63% of the DEmiRs were down-regulated in CTN-treated sample as compared to the control. However, over 88% of the DEmiRs (Fig. 3b and c) was found to be up-regulated in OTA-treated samples. These miRNAs data are generally corresponded with the transcriptome data (Fig. 2), in which CTN treatment induced more expression of genes while OTA treatment imposed a wider inhibitory effect on gene expression, as compared to the control. A Venn diagram of those DEmiRs in multiple comparisons showed both common and specific miRNAs affected (Fig. 3d). It was also worth noting that the number of DEmiRs in OTA-treated sample was three times more than that in CTN-treated sample, correlating well with that a larger number of DEGs were identified from transcriptome sequencing in OTA-treated than that in CTN-treated samples (Fig. 2). Of the eight DEmiRs identified from different treatment protocols, five (miR-122–5p, miR-1246, miR-1290, miR-215–5p and miR-7-5p) were found to be significantly up-regulated by CTN- or OTA-treatment alone and CTN/OTA co-treatments, while only hsa-miR-1268a was down-regulated by all treatment protocols. Interestingly, hsa-miR-1-3p and hsa-miR-34c-5p showed an inconsistent expression change upon different treatments, where both were repressed by CTN- treatment but induced by OTA treatment alone or CTN/OTA co-treatment (Fig. 3a). These results suggested that different mycotoxins might have imposed their effects via different miRNA-mediated pathways.

3.7. Targets of differential miRNAs upon mycotoxin treatment

Compared with plant miRNAs, the complementarity between mature miRNAs and target transcripts in animals was commonly less stringent. Hence, animal miRNAs can potentially target hundreds of different mRNAs, thus regulating a wide variety of cellular processes (Krol et al., 2010). Using TargetScan, miRDB and miRanda algorithms, we predicted the target genes of all the identified miRNAs in our study, and retained 28 miRNAs with targets independently predicted via at least two algorithms. Among these, 1148 targets were further obtained for the nine DEmiRs upon mycotoxin treatment (Table S11). The number of the predicted targets greatly varied for different miRNAs, ranging from six targets for hsa-miR-107 to 337 targets for hsa-miR-1290 (Table S11). Some miRNAs shared same targets. For example, a polypeptide N-acetylgalactosaminyltransferase gene was co-targeted by hsa-miR-122–5p, hsa-miR-1290 and hsa-miR-139–5p; a vesicle trafficking protein gene was co-targeted by hsa-miR-122–5p, hsa-miR-1246 and hsa-miR-1290; an arrestin domain containing protein gene was also co-targeted by hsa-miR-1290, hsa-miR-139–5p and hsa-miR-32–5p. GO enrichment analysis was conducted for all of these target genes to identify which GO terms are over-represented or under-represented (Table S12). While most GO terms related to cellular process were over-represented, a group of specific GO categories involved in 'sensory perception' was significantly under-represented ($p < 0.0001$), suggesting that the sensory perception of the cells had been significantly deactivated upon mycotoxin treatment. After manually checking transcriptome and the predicted target gene data, we further found that programmed cell death protein 10 (*PDCD10*) and Cyclin G1 (*CCNG1*) involving apoptotic and cell cycle processes, were both within the corresponding enriched GO terms (Table S11).

3.8. Expression validation of PDCD10 and CCNG1

Transcriptome analysis showed that *PDCD10* was significantly down-regulated by OTA treatment and *CCNG1* was also significantly down-regulated by CTN/OTA co-treatment, which were further confirmed by qPCR (Fig. 4a). Western blot analysis detected a lower CCNG1 protein level in CTN-treated and CTN/OTA co-treated sample, while a significantly decreased level of PDCD10 protein was observed in OTA-treated samples, further confirming the inhibitory effect of hsa-miR-1-3p and hsa-miR-122–5p on their corresponding targets at the protein levels (Fig. 4b).

3.9. Validation of PDCD10 and CCNG1 as selected miRNA targets involved in apoptosis and cell cycle

Based on the bioinformatics prediction, *PDCD10* and *CCNG1* genes were targeted by hsa-miR-1-3p and hsa-miR-122–5p, respectively. MiRNA sequencing data showed that both hsa-miR-1-3p and hsa-miR-122–5p were greatly induced by OTA-treatment and CTN/OTA co-treatment, which were further confirmed by qPCR (Fig. 5a). It is inversely corresponded to the expression pattern of their target genes. Therefore, these two miRNA-target pairs were selected for further experimental validation.

Dual-luciferase reporter gene assay showed that hsa-miR-122–5p could effectively target wide-type mRNA 3′-UTR of *CCNG1*, causing a 48% reduction in the fluorescence intensity. However, such an inhibition was reversed lost in the *CCNG1* mimic assay with mutated target sites (Fig. 5b). In addition, hsa-miR-1-3p combined specifically with wide-type mRNA 3′-UTR of *PDCD10*, and inhibited the luciferase activity by 54.6% ($p < 0.05$). The inhibition of hsa-miR-1-3p was partially released when the target region of 'ACATTCC' was mutated to 'TGTAAGG' on *PDCD10* 3'-UTR (Fig. 5c). Overall, the qPCR and RNA-sequencing data corresponded well in terms of the expression patterns of hsa-miR-1-3p and hsa-miR-122–5p (Fig. 5a).

4. Discussion

OTA, one of the most abundant mycotoxin, is a common food contaminant, which imposes toxic effect on human and animals via dietary exposure. OTA often occurs together with CTN in food and feed, and their toxic effects of co-occurrence are either additive or synergistic, for example, in human proximal tubule-derived cells (Schulz et al., 2018). In this study a significant synergistic cytotoxic effect of co-treatment with OTA and CTN in HEK293 cells was found with the EC_{50} as low as 7 μM (Fig. 1), which is consistent with previous report on renal cells (Bouslimi et al., 2008). Although, both mycotoxins in such high concentrations may never occur during natural contamination, it has been demonstrated that co-contamination with OTA and CTN was common in wheat and barley because the toxigenic *P. verrucosum* can naturally produce both mycotoxins, and therefore, co-exposure to OTA and CTN may play a synergistic role in causing human nephrotoxicity (Lund and Frisvad, 2003; Schmidt-Heydt et al., 2015). It was found that OTA could induce cell cycle arrest at the S phase, while CTN induced G2/M arrest in human embryonic kidney (HEK293) cells (Chang et al., 2011; Yang et al., 2014), and our results were fully agreed with these reports, but further revealed that the co-treatment with OTA and CTN could induce cell cycle arrest at both S and G2/M phase, suggesting that combinative effects of OTA and CTN are clearly synergistic.

OTA has been classified as a class 2B human carcinogen with confirmed carcinogenic effects in animal studies, while co-treatment with CTN reduced OTA induced carcinogenicity (IARC, 1993). Our transcriptomic data showed that much more genes altered their expressions in the OTA-treated samples as compared to CTN-treated samples, suggesting that OTA has more potent toxic effects. Differences in toxicity between OTA and CTN are also obvious, Vanacloig-Pedros et al. (2016) reported that CTN and OTA induced largely separated gene sets in yeast, and CTN mainly caused the rapid induction of antioxidant and drug extrusion-related gene functions, but OTA mainly deregulated developmental genes associated with yeast sporulation and sexual reproduction. However, our high-throughput experiments clearly suggested that both PCD and cell cycle were universal biological process regulated by individual and combinative treatments with OTA and CTN in HEK293 cells, which is consistent with a general knowledge that these two mycotoxins can influence cell proliferation and death in various organisms, including regulation of cell cycle progression and PCD (Alshannaq and Yu, 2017; Dutto et al., 2015).

We found that expression of all the apoptosis-related genes were commonly up-regulated in response to CTN-treatment, while OTA-

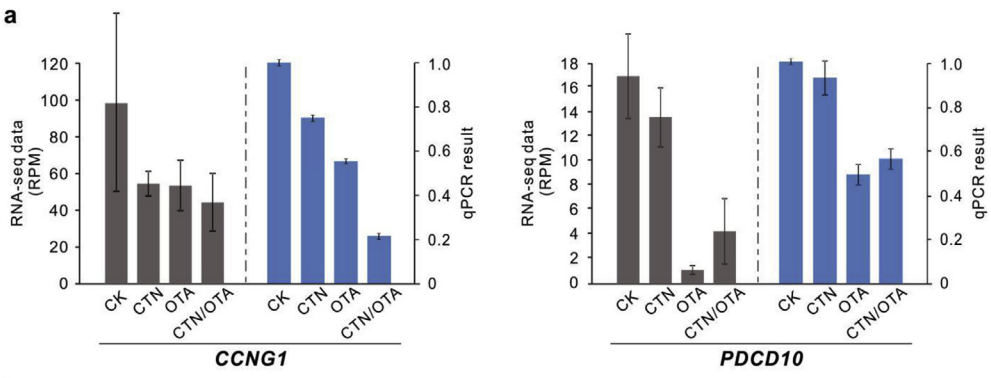

Fig. 4. Validation of miRNA-target interaction at both transcript and protein levels. (a) Transcript levels of *CCNG1* and *PDCD10* between RNA-seq data and real-time quantitative PCR assay upon toxin treatment. (b) Western blot showing reduced levels of corresponding proteins upon different toxin treatments (red boxes). (For interpretation of the references to colour in this figure legend, the reader is referred to the Web version of this article.)

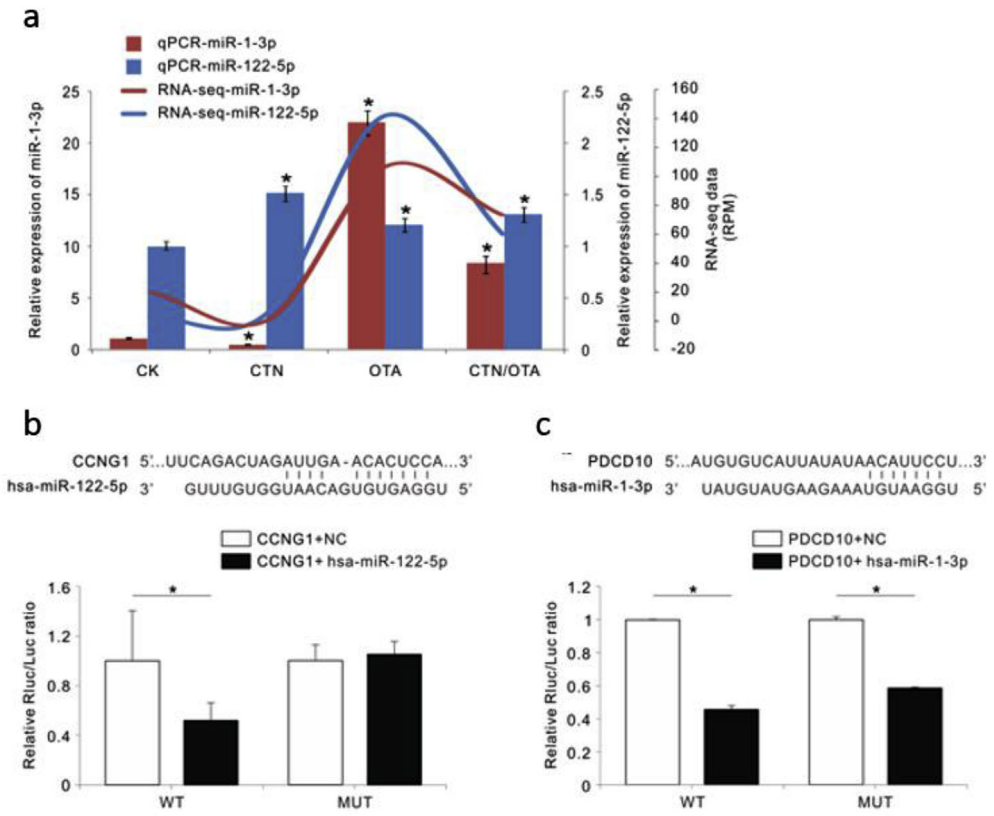

Fig. 5. (a–b) Dual-luciferase reporter assay for the validation of the effect of miR-1-3p and miR-122–5p on their corresponding target genes. (c) Correlation of the expression of miR-1-3p and miR-122–5p between RNA-seq data and real-time quantitative PCR assay.

treatment inhibited expression of these genes, and co-treatment with OTA and CTN reserved the inhibitory effect (Table S5). Previous research reported that CTN under *in vivo* condition caused apoptosis through the mitochondria-mediated pathway in mouse skin (Kumar et al., 2011). The cytotoxicity of CTN may be triggered by its ability to induce apoptosis in embryonic stem cells (Yu et al., 2006). TNF had the ability to induce apoptosis in a wide variety of transformed cell lines (Wiley et al., 1995), and TNFR can promote TNF to transduce the signal needed for apoptotic activity (Vilcek and Lee, 1991). Therefore, high expression of TNFR in CTN-treated cell (Fig. S2) suggests that apoptosis process is induced by CTN-treatment. Autophagy is another type of programmed cell death, which is linked with type II (non-apoptotic) programmed cell death and may contribute to death in cells (Xue et al., 1999). In this study, autophagy related-gene such as autophagy related 4D (*ATG4D*) and Fas (TNFRSF6)-associated via death domain (*FADD*) were down-regulated under the exposure to OTA. The inhibition of these autophagy-related genes by OTA in the present study suggests that autophagy process might be alleviated in OTA-treated cell. Overall, our data indicate that CTN-treatment can induce PCD process while OTA-treatment can alleviate this process.

Cell cycle-related genes showed different expression patterns in response to different treatment protocols in our transcriptomic data

(Table S6). OTA can induce karyomegaly and cell cycle aberrations in renal tubular cells of rats (Taniai et al., 2014). Induction of cell cycle progression was found to be a main contributing factor for CTN-induced renal carcinogenesis in the kidneys of rats (Kuroda et al., 2013). Cell-division cycle (*CDC*) proteins are of importance for division and DNA replication in the eukaryote cells (Kapanidou et al., 2017; Petojevic et al., 2015). In the present study, expression of seven *CDC* homologues were significantly changed in HEK293 cells under the different treatment protocol. Interestingly, *CDC25A* was down-regulated by OTA treatment, while up-regulated in CTN-treated samples, which may partly explain our finding why OTA resulted in cell cycle arrest in the S phase, but CTN caused G2/M arrest. It was found that overexpression of *CDC 25A* accelerates human cells entry into mitosis, while CDC25A-deficient cells were failure to prematurely enter mitosis (Mazzolini et al., 2016; Ruiz et al., 2016). It is well known that the eukaryotic cell cycle is regulated by cyclin-dependent protein kinases (CDKs) and their activities are controlled by cyclins and CDK inhibitors (Malumbres et al., 2009). Our study show that CTN-treatment decreased the *CDKN1B* expression level in HEK293 cells, but expression of *CDKN1B* and *CDKN2A* were up-regulated in OTA-treated cells (Fig. S2). This may also explain why OTA and CTN led to S and G2/M arrest, because M and G2 phases required much higher CDK activity than G1 and S phases (Harashima et al., 2013).

Previous studies have revealed that OTA can induce carcinogenicity and mutagenicity possibly via oxidative DNA damage (Palma et al., 2007). OTA exposure resulted in onset/progression of porcine nephrotoxicity, although the nephrotoxic effects may require synergistic interactions with predisposing genotypes or other environmental toxicants (Abouzied et al., 2002). CTN usually co-exists with OTA in stored grains, sometimes also in fruits and vegetables. Although many studies emphasized on the molecular mechanism of toxic effects caused by OTA and CTN, the involvement of miRNA in the toxic mechanism has received little attention. OTA was shown to impair miRNA biogenesis in the kidneys of affected rats (Dai et al., 2014). miR-129 played an important role in regulating cell proliferation by downregulation of Cdk6 (Wu et al., 2010). It has also been reported that miR-99a could induce cell cycle arrest and suppress tumorigenesis, and miR-133b enhanced apoptosis in HeLa cells (Cui et al., 2012; Patron et al., 2012). While these findings reveal potential roles of miRNAs in toxicity, more direct evidence that miRNAs mediate mycotoxin-induced cell responses is still insufficient. Moreover, it remains unclear if different mycotoxins, like single or mixture of OTA and CTN, drive toxic responses via different miRNA-mediated pathways.

Based on previous toxicological studies on OTA and CTN, we hypothesized that both toxins may jointly or individually induce the abnormal expression of specific miRNAs, leading to disorders in cell function, thus contributing to mycotoxin-induced nephrotoxicity. To test this hypothesis, we compared the high-throughput profiles of miRNA in normal and OTA and CTN-treated HEK293 cells. Totally, we identified 378 miRNAs from all cell samples and generated a differential miRNA expression profile in HEK293 cells received different treatment protocols (control, OTA-treatment, CTN-treatment and OTA/CTN-co-treatment). CTN-treatment significantly suppressed most differentially expressed miRNAs, but OTA-treatment significantly induced over 80% of differential miRNAs (Table S10), indicating that these two mycotoxins have driven divergent miRNA-mediated pathways. The results of the microRNA expression are consistent with the transcriptome data that CTN increased the expression of most DEGs, while OTA decreased them. GO analysis combining miRNA targetome with transcriptome revealed substantially enriched categories involved in cell growth and cell death (Table S11). Genes on these categories were mainly targeted by six differentially expressed miRNAs, including hsa-miR-1290, hsa-miR-139–5p, hsa-miR-32–5p, miR-122–5p, miR-1246 and hsa-miR-1-3p, which confirmed the linkage between cell function and nephrotoxicity bridged by miRNAs.

It has been demonstrated that evolutionarily conserved miRNAs usually have more abundant expression than newly evolved miRNAs. It was reported that miR-122, related to hepatitis C virus infection, was down-regulated after pathogen infection, but still remained at a high level (Gramantieri et al., 2007). Our sequencing results confirmed that most conserved miRNAs were highly expressed except for the miR-122–5p, which was marginally expressed in the control sample but significantly up-regulated after mycotoxin treatment, especially by OTA (Fig. 5). CyclinG1 (*CCNG1*) is a target of the liver-specific miR-122 (Gramantieri et al., 2007) which was also targeted by miR-122–5p in our study and there was an inverse correlation link between miR-122–5p and *CCNG1* expression in OTA/CTN co-treatment (Figs. 4 and 5). Similarly, Chen et al. (2015) reported that miR-122 partly mediates the OTA-induced GC-2 cell apoptosis. These findings further suggest that miR-122-*CCNG1* regulatory circuit plays a critical role in the cell cycle control of mycotoxin-induced nephrotoxicity.

Among the differentially expressed miRNAs, we found that miR-1-3p was greatly down-regulated by CTN but up-regulated by OTA and OTA/CTN co-treatments. The target of miR-1-3p is programmed cell death 10 (*PDCD10*), which was initially identified to be associated with cell apoptosis. PDCD10 was found to interact with a kinase MST4 to promote cell proliferation and transformation (Ma et al., 2007). In our study both *PDCD10* transcript and protein levels were greatly suppressed by OTA-treatment, likely via the elevated miR-1-3p level (Figs. 4 and 5). Similar expression patterns to miR-1-3p were also observed for miR-34c-5p and miR-139 (Table S10). A recent study found that miR-34a negatively regulates the expression of Wnt/β-catenin signaling pathway in Aflatoxin B_1-induced hepatotoxicity (Zhu et al., 2015). Although no direct target had been experimentally validated for miR-34c-5p, the potential role of miR-34 family awaits further investigation.

In conclusion, co-exposure to CTN and OTA induced more potent cytotoxicity than that induced by exposure to either mycotoxin alone. sRNA sequencing revealed 66 miRNAs targeting thousands of genes which were differentially expressed in response to different treatment protocols. Transcriptome data showed that CTN induced more gene expressions while OTA imposed a wider inhibitory effect on gene expression. These findings showed molecular signatures for cytotoxic effects of CTN and OTA on HEK293 cells. In addition, GO analysis of the transcriptome data revealed that PCD and cell cycle are the tightly regulated biological processes in HEK293 under two mycotoxin treatment protocols. Herein hsa-miR-1-3p and hsa-miR-122–5p played important roles in OTA and CTN-induced apoptosis and cell cycle arrest through regulating the expression of their target genes, i.e. *PDCD10* and *CCNG1*, which triggered further cytotoxic effects (Fig. 6).

Conflicts of interest

The authors declare that there are no conflicts of interest.

Acknowledgements

This research was supported by the National Natural Science Foundation of China (No. 31772033, 31401593, 31772371 and 31772041), the Science and Technology Planning Project of Guangzhou (Nos. 201710010135, 201804020041 and 201604020048), the Science and Technology Planning Project of Guangdong Province (No. 2015B090901058), and Talent Program of Guangdong Province (No. 2014TX01N049). The work also was supported by Key Laboratory of Plant Resource Conservation and Sustainable Utilization, CAS.

Transparency document

Transparency document related to this article can be found online at https://doi.org/10.1016/j.fct.2018.11.015.

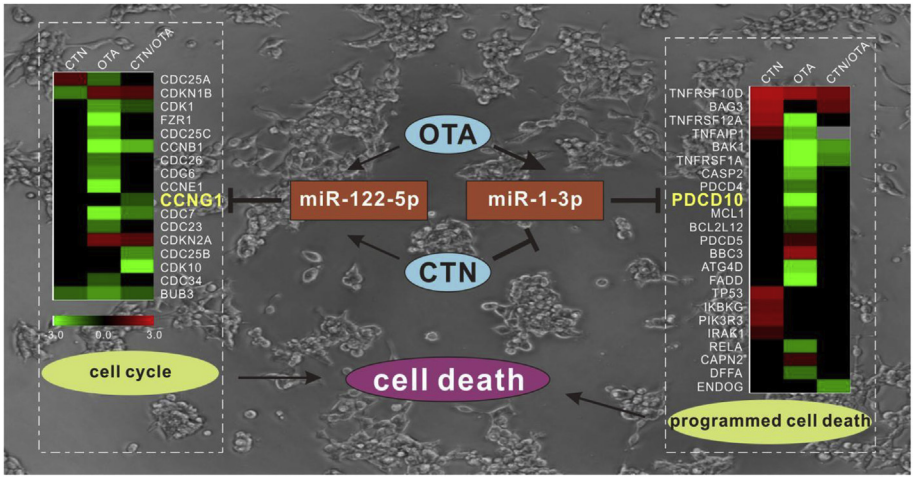

Fig. 6. A proposed mechanism of nephrotoxicity induced by CTN and OTA through miRNAs in HEK293 cells. OTA strongly induced the expression of hsa-miR-1-3p, which was although slightly inhibited by CTN, thus *PDCD10*, the target of hsa-miR-1-3p was down-regulated in OTA-treated samples. On the other hand, hsa-miR-122–5p was collectively induced by CTN and OTA, so its induction strengthened the inhibitory effect on its target *CCNG1*, which impeded the cell cycle. Background picture is the morphology of HEK293 cells under the mycotoxins treatment.

Appendix A. Supplementary data

Supplementary data to this article can be found online at https://doi.org/10.1016/j.fct.2018.11.015.

References

Abouzied, M.M., Horvath, A.D., Podlesny, P.M., Regina, N.P., Metodiev, V.D., Kamenova-Tozeva, R.M., Niagolova, N.D., Stein, A.D., Petropoulos, E.A., Ganev, V.S., 2002. Ochratoxin A concentrations in food and feed from a region with Balkan Endemic Nephropathy. Food Addit. Contam. 19, 755–764.

Alshannaq, A., Yu, J.-H., 2017. Occurrence, toxicity, and analysis of major mycotoxins in food. Int. J. Environ. Res. Publ. Health 14.

Bartel, D.P., 2009. MicroRNAs: target recognition and regulatory functions. Cell 136, 215–233.

Berridge, M.V., Herst, P.M., Tan, A.S., 2005. Tetrazolium dyes as tools in cell biology: new insights into their cellular reduction. Biotechnol. Annu. Rev. 11, 127–152.

Bouslimi, A., Bouaziz, C., Ayed-Boussema, I., Hassen, W., Bacha, H., 2008. Individual and combined effects of ochratoxin A and citrinin on viability and DNA fragmentation in cultured Vero cells and on chromosome aberrations in mice bone marrow cells. Toxicology 251, 1–7.

Chang, C.-H., Yu, F.-Y., Wu, T.-S., Wang, L.-T., Liu, B.-H., 2011. Mycotoxin citrinin induced cell cycle G2/M arrest and numerical chromosomal aberration associated with disruption of microtubule formation in human cells. Toxicol. Sci. 119, 84–92.

Chen, R., Deng, L., Yu, X., Wang, X., Zhu, L., Yu, T., Zhang, Y., Zhou, B., Xu, W., Chen, L., Luo, H., 2015. MiR-122 partly mediates the ochratoxin A-induced GC-2 cell apoptosis. Toxicol. Vitro 30, 264–273.

Cui, L., Zhou, H., Zhao, H., Zhou, Y., Xu, R., Xu, X., Zheng, L., Xue, Z., Xia, W., Zhang, B., Ding, T., Cao, Y., Tian, Z., Shi, Q., He, X., 2012. MicroRNA-99a induces G1-phase cell cycle arrest and suppresses tumorigenicity in renal cell carcinoma. BMC Canc. 12, 546.

Dai, Q., Zhao, J., Qi, X., Xu, W., He, X., Guo, M., Dweep, H., Cheng, W.-H., Luo, Y., Xia, K., Gretz, N., Huang, K., 2014. MicroRNA profiling of rats with ochratoxin A nephrotoxicity. BMC Genomics 15, 333.

Dai, X., Zhao, P.X., 2011. psRNATarget: a plant small RNA target analysis server. Nucleic Acids Res. 39, W155–W159.

de Oliveira Filho, J.W.G., Islam, M.T., Ali, E.S., Uddin, S.J., Santos, J.V.O., de Alencar, M.V.O.B., et al., 2017. A comprehensive review on biological properties of citrinin. Food Chem. Toxicol. 110, 130–141.

Donmez-Altuntas, H., Dumlupinar, G., Imamoglu, N., Hamurcu, Z., Liman, B.C., 2007. Effects of the mycotoxin citrinin on micronucleus formation in a cytokinesis-block genotoxicity assay in cultured human lymphocytes. J. Appl. Toxicol. 27, 337–341.

Dutto, I., Tillhon, M., Cazzalini, O., Stivala, L.A., Prosperi, E., 2015. Biology of the cell cycle inhibitor p21(CDKN1A): molecular mechanisms and relevance in chemical toxicology. Arch. Toxicol. 89, 155–178.

Fahlgren, N., Howell, M.D., Kasschau, K.D., Chapman, E.J., Sullivan, C.M., Cumbie, J.S., Givan, S.A., Law, T.F., Grant, S.R., Dangl, J.L., Carrington, J.C., 2007. High-throughput sequencing of arabidopsis microRNAs: evidence for frequent birth and death of MIRNA genes. PloS One 2 (2), e219.

Farabegoli, F., Scarpa, E.S., Frati, A., Serafini, G., Papi, A., Spisni, E., Antonini, E., Benedetti, S., Ninfali, P., 2017. Betalains increase vitexin-2-O-xyloside cytotoxicity in CaCo-2 cancer cells. Food Chem. 218, 356–364.

Friedlaender, M.R., Mackowiak, S.D., Li, N., Chen, W., Rajewsky, N., 2012. miRDeep2 accurately identifies known and hundreds of novel microRNA genes in seven animal clades. Nucleic Acids Res. 40, 37–52.

Gayathri, L., Dhivya, R., Dhanasekaran, D., Periasamy, V.S., Alshatwi, A.A., Akbarsha, M.A., 2015. Hepatotoxic effect of ochratoxin A and citrinin, alone and in combination, and protective effect of vitamin E: in vitro study in HepG2 cell. Food Chem. Toxicol. 83, 151–163.

Gramantieri, L., Ferracin, M., Fornari, F., Veronese, A., Sabbioni, S., Liu, C.-G., Calin, G.A., Giovannini, C., Ferrazzi, E., Grazi, G.L., Croce, C.M., Bolondi, L., Negrini, M., 2007. Cyclin g1 is a target of miR-122a, a MicroRNA frequently down-regulated in human hepatocellular carcinoma. Cancer Res. 67, 6092–6099.

Harashima, H., Dissmeyer, N., Schnittger, A., 2013. Cell cycle control across the eukaryotic kingdom. Trends Cell Biol. 23, 345–356.

Heussner, A.H., Bingle, L.E.H., 2015. Comparative ochratoxin toxicity: a review of the available data. Toxins 7, 4253–4282. https://doi.org/10.3390/toxins7104253.

Huang, Z., Lu, Z., Tian, J., Wang, G., Gao, Z., 2015. Effect of a functional polymorphism in the pre-miR-146a gene on the risk and prognosis of renal cell carcinoma. Mol. Med. Rep. 12, 6997–7004.

Huntley, R.P., Sawford, T., Mutowo-Meullenet, P., Shypitsyna, A., Bonilla, C., Martin, M.J., O'Donovan, C., 2015. The Goa database: gene ontology annotation updates for 2015. Nucleic Acids Res. 43, D1057–D1063.

International Agency For Research On Cancer, 1993. IARC monographs on the evaluation of carcinogenic risks to humans. In: International Agency For Research On Cancer (Ed.), Some Naturally Occurring Substances: Food Items and Constituents, Heterocyclic Aromatic Amines and Mycotoxins. International Agency for Research on Cancer (IARC), Lyon 599p-599p.

Kanehisa, M., Furumichi, M., Tanabe, M., Sato, Y., Morishima, K., 2017. KEGG: new perspectives on genomes, pathways, diseases and drugs. Nucleic Acids Res. 45, D353–D361.

Kapanidou, M., Curtis, N.L., Bolanos-Garcia, V.M., 2017. Cdc20: at the crossroads between chromosome segregation andmitotic exit. Trends Biochem. Sci. 42, 193–205.

Klaric, M.S., Medic, N., Hulina, A., Grubisic, T.Z., Rumora, L., 2014. Disturbed Hsp70 and Hsp27 expression and thiol redox status in porcine kidney PK15 cells provoked by individual and combined ochratoxin A and citrinin treatments. Food Chem. Toxicol. 71, 97–105.

Krol, J., Loedige, I., Filipowicz, W., 2010. The widespread regulation of microRNA biogenesis, function and decay. Nat. Rev. Genet. 11, 597–610.

Kumar, M., Dwivedi, P., Sharma, A.K., Sankar, M., Patil, R.D., Singh, N.D., 2014. Apoptosis and lipid peroxidation in ochratoxin A- and citrinin-induced nephrotoxicity in rabbits. Toxicol. Ind. Health 30 (1), 90–98.

Kumar, M., Dwivedi, P., Sharma, A.K., Singh, N.D., Patil, R.D., 2007. Ochratoxin A and citrinin nephrotoxicity in New Zealand White rabbits: an ultrastructural assessment. Mycopathologia 163, 21–30.

Kumar, R., Dwivedi, P.D., Dhawan, A., Das, M., Ansari, K.M., 2011. Citrinin-generated reactive oxygen species cause cell cycle arrest leading to apoptosis via the intrinsic mitochondrial pathway in mouse skin. Toxicol. Sci. 122, 557–566.

Kuroda, K., Ishii, Y., Takasu, S., Kijima, A., Matsushita, K., Watanabe, M., Takahashi, H., Sugita-Konishi, Y., Sakai, H., Yanai, T., Nohmi, T., Ogawa, K., Umemura, T., 2013. Cell cycle progression, but not genotoxic activity, mainly contributes to citrinin-induced renal carcinogenesis. Toxicology 311, 216–224.

Langmead, B., Trapnell, C., Pop, M., Salzberg, S.L., 2009. Ultrafast and memory-efficient alignment of short DNA sequences to the human genome. Genome Biol. 10.

Li, Y., Zhang, Z., Liu, F., Vongsangnak, W., Jing, Q., Shen, B., 2012. Performance comparison and evaluation of software tools for microRNA deep-sequencing data analysis. Nucleic Acids Res. 40, 4298–4305.

Livak, K.J., Schmittgen, T.D., 2001. Analysis of relative gene expression data using real-time quantitative PCR and the 2(T)(-Delta Delta C) method. Methods 25, 402–408.

Love, M.I., Huber, W., Anders, S., 2014. Moderated estimation of fold change and dispersion for RNA-seq data with DESeq2. Genome Biol. 15 (12), 550.

Lund, F., Frisvad, J.C., 2003. Penicillium verrucosum in wheat and barley indicates presence of ochratoxin A. J. Appl. Microbiol. 95, 1117–1123.

Ma, X., Zhao, H.-S., Ma, D.-L., 2007. Programmed cell death 10, beyond an apoptosis-related molecule. Prog. Biochem. Biophys. 34, 781–790.

Malir, F., Ostry, V., Pfohl-Leszkowicz, A., Malir, J., Toman, J., 2016. Ochratoxin A: 50 years of research. Toxins 8 (7), 191.

Malumbres, M., Harlow, E., Hunt, T., Hunter, T., Lahti, J.M., Manning, G., Morgan, D.O., Tsai, L.-H., Wolgemuth, D.J., 2009. Cyclin-dependent kinases: a family portrait. Nat. Cell Biol. 11, 1275–1276.

Mazzolini, L., Broban, A., Froment, C., Burlet-Schiltz, O., Besson, A., Manenti, S., Dozier, C., 2016. Phosphorylation of CDC25A on SER283 in late S/G2 by CDK/cyclin complexes accelerates mitotic entry. Cell Cycle 15, 2742–2752.
Ostry, V., Malir, F., Ruprich, J., 2013. Producers and important dietary sources of ochratoxin A and citrinin. Toxins 5, 1574–1586.
Palma, N., Cinelli, S., Sapora, O., Wilson, S.H., Dogliotti, E., 2007. Ochratoxin A-induced mutagenesis in mammalian cells is consistent with the production of oxidative stress. Chem. Res. Toxicol. 20, 1031–1037.
Patron, J.P., Fendler, A., Bild, M., Jung, U., Mueller, H., Arntzen, M.O., Piso, C., Stephan, C., Thiede, B., Mollenkopf, H.-J., Jung, K., Kaufmann, S.H.E., Schreiber, J., 2012. MiR-133b targets antiapoptotic genes and enhances death receptor-induced apoptosis. PloS One 7 (4), e35345.
Petojevic, T., Pesavento, J.J., Costa, A., Liang, J., Wang, Z., Berger, J.M., Botchan, M.R., 2015. Cdc45 (cell division cycle protein 45) guards the gate of the Eukaryote Replisome helicase stabilizing leading strand engagement. Proc. Natl. Acad. Sci. U. S. A 112, E249–E258.
Pflaum, T., Hausler, T., Baumung, C., Ackermann, S., Kuballa, T., Rehm, J., Lachenmeier, D.W., 2016. Carcinogenic compounds in alcoholic beverages: an update. Arch. Toxicol. 90, 2349–2367.
Pleadin, J., Zadravec, M., Lešić, T., Vahčić, N., Frece, J., Mitak, M., Markov, K., 2018. Co-occurrence of ochratoxin A and citrinin in unprocessed cereals established during a three-year investigation period. Food Addit. Contam. Part B Surveill. 11 (1), 20–25.
Reddy, L., Bhoola, K., 2010. Ochratoxins-food contaminants: impact on human health. Toxins 2, 771–779.
Ruiz, S., Mayor-Ruiz, C., Lafarga, V., Murga, M., Vega-Sendino, M., Ortega, S., Fernandez-Capetillo, O., 2016. A genome-wide CRISPR screen identifies CDC25A as a determinant of sensitivity to ATR inhibitors. Mol. Cell. 62, 307–313.
Saraiva, C., Esteves, M., Bernardino, L., 2017. MicroRNA: basic concepts and implications for regeneration and repair of neurodegenerative diseases. Biochem. Pharmacol. 141, 118–131.
Schilter, B., Marin-Kuan, M., Delatour, T., Nestler, S., Mantle, P., Cavin, C., 2005. Ochratoxin A: potential epigenetic mechanisms of toxicity and carcinogenicity. Food Addit. Contam. 22, 88–93.
Schmidt-Heydt, M., Stoll, D., Schuetz, P., Geisen, R., 2015. Oxidative stress induces the biosynthesis of citrinin by *Penicillium verrucosum* at the expense of ochratoxin. Int. J. Food Microbiol. 192, 1–6.
Schulz, M.C., Schumann, L., Rottkord, U., Humpf, H.U., Gekle, M., Schwerdt, G., 2018. Synergistic action of the nephrotoxic mycotoxins ochratoxin A and citrinin at nanomolar concentrations in human proximal tubule-derived cells. Toxicol. Lett. 291, 149–157.
Supek, F., Bosnjak, M., Skunca, N., Smuc, T., 2011. REVIGO summarizes and visualizes long lists of gene ontology terms. PloS One 6.
Taniai, E., Yafune, A., Nakajima, M., Hayashi, S.-M., Nakane, F., Itahashi, M., Shibutani, M., 2014. Ochratoxin A induces karyomegaly and cell cycle aberrations in renal tubular cells without relation to induction of oxidative stress responses in rats. Toxicol. Lett. 224, 64–72.
Tao, Y., Xie, S., Xu, F., Liu, A., Wang, Y., Chen, D., Pan, Y., Huang, L., Peng, D., Wang, X., Yuan, Z., 2018. Ochratoxin A: toxicity, oxidative stress and metabolism. Food Chem. Toxicol. 112, 320–331.
Vanacloig-Pedros, E., Proft, M., Pascual-Ahuir, A., 2016. Different toxicity mechanisms for citrinin and ochratoxin A revealed by transcriptomic analysis in yeast. Toxins 8.
Verma, P., Shah, N., Bhatia, S., 2013. Development of an expressed gene catalogue and molecular markers from the de novo assembly of short sequence reads of the lentil (*Lens culinaris* Medik.) transcriptome. Plant Biotechnol. J. 11, 894–905.
Vidigal, J.A., Ventura, A., 2015. The biological functions of miRNAs: lessons from in vivo studies. Trends Cell Biol. 25 (3), 137–147.
Vilcek, J., Lee, T.H., 1991. Tumor-necrosis-factro-new insights into the molecular mechanisms of its multiple actions. J. Biol. Chem. 266, 7313–7316.
Wawrzyniak, J., Waskiewicz, A., 2014. Ochratoxin A and citrinin production by *Penicillium verrucosum* on cereal solid substrates. Food Addit. Contam. Part A Chem. Anal. Control Expo. Risk Assess 31, 139–148.
Wiley, S.R., Schooley, K., Smolak, P.J., Din, W.S., Huang, C.P., Nicholl, J.K., Sutherland, G.R., Smith, T.D., Rauch, C., Smith, C.A., Goodwin, R.G., 1995. Identification and characterization of a new member of the TNF family that induces apoptosis. Immunity 3, 673–682.
Wu, J., Qian, J., Li, C., Kwok, L., Cheng, F., Liu, P., Perdomo, C., Kotton, D., Vaziri, C., Anderlind, C., Spira, A., Cardoso, W.V., Lue, J., 2010. miR-129 regulates cell proliferation by downregulating Cdk6 expression. Cell Cycle 9, 1809–1818.
Wu, Q., Dohnal, V., Huang, L., Kuca, K., Wang, X., Chen, G., Yuan, Z., 2011. Metabolic pathways of ochratoxin A. Curr. Drug Metabol. 12, 1–10.
Xue, L.Z., Fletcher, G.C., Tolkovsky, A.M., 1999. Autophagy is activated by apoptotic signalling in sympathetic neurons: an alternative mechanism of death execution. Mol. Cell. Neurosci. 14, 180–198.
Yang, Q., He, X., Li, X., Xu, W., Luo, Y., Yang, X., Wang, Y., Li, Y., Huang, K., 2014. DNA damage and S phase arrest induced by Ochratoxin A in human embryonic kidney cells (HEK 293). Mutat. Res. 765, 22–31.
Yang, X., Li, L., 2011. miRDeep-P: a computational tool for analyzing the microRNA transcriptome in plants. Bioinformatics 27, 2614–2615.
Yu, F.Y., Liao, Y.C., Chang, C.H., Liu, B.H., 2006. Citrinin induces apoptosis in HL-60 cells via activation of the mitochondrial pathway. Toxicol. Lett. 161, 143–151.
Zhang, Y., Qi, X., Zheng, J., Luo, Y., Huang, K., Xu, W., 2016. High-throughput tag-sequencing analysis of early events induced by ochratoxin A in HepG-2 cells. J. Biochem. Mol. Toxicol. 30, 29–36.
Zhu, L., Gao, J., Huang, K., Luo, Y., Zhang, B., Xu, W., 2015. miR-34a screened by miRNA profiling negatively regulates Wnt/beta-catenin signaling pathway in Aflatoxin B1 induced hepatotoxicity. Sci. Rep. 5, 16732.